Distinct roles for motor neuron autophagy early and late in the SOD1^{G93A} mouse model of ALS

Noam D. Rudnick[a,b], Christopher J. Griffey[c], Paolo Guarnieri[d], Valeria Gerbino[c], Xueyong Wang[e,f], Jason A. Piersaint[c], Juan Carlos Tapia[b,1], Mark M. Rich[e,f], and Tom Maniatis[c,g,2]

[a]College of Physicians and Surgeons, Columbia University, New York, NY 10032; [b]Department of Neuroscience, Columbia University Medical Center, New York, NY 10032; [c]Department of Biochemistry and Molecular Biophysics, Columbia University Medical Center, New York, NY 10032; [d]Department of Systems Biology, Herbert Irving Comprehensive Cancer Center, Columbia University Medical Center, New York, NY 10032; [e]Department of Neurology, Wright State University, Dayton, OH 45435; [f]Department of Neuroscience, Cell Biology and Physiology, Wright State University, Dayton, OH 45435; and [g]Mortimer B. Zuckerman Mind Brain Behavior Institute, Columbia University, New York, NY 10032

Contributed by Tom Maniatis, August 8, 2017 (sent for review March 17, 2017; reviewed by Virginia Lee and Leonard Petrucelli)

Mutations in autophagy genes can cause familial and sporadic amyotrophic lateral sclerosis (ALS). However, the role of autophagy in ALS pathogenesis is poorly understood, in part due to the lack of cell type-specific manipulations of this pathway in animal models. Using a mouse model of ALS expressing mutant superoxide dismutase 1 (SOD1^{G93A}), we show that motor neurons form large autophagosomes containing ubiquitinated aggregates early in disease progression. To investigate whether this response is protective or detrimental, we generated mice in which the critical autophagy gene *Atg7* was specifically disrupted in motor neurons (Atg7 cKO). Atg7 cKO mice were viable but exhibited structural and functional defects at a subset of vulnerable neuromuscular junctions. By crossing Atg7 cKO mice to the SOD1^{G93A} mouse model, we found that autophagy inhibition accelerated early neuromuscular denervation of the tibialis anterior muscle and the onset of hindlimb tremor. Surprisingly, however, lifespan was extended in Atg7 cKO; SOD1^{G93A} double-mutant mice. Autophagy inhibition did not prevent motor neuron cell death, but it reduced glial inflammation and blocked activation of the stress-related transcription factor c-Jun in spinal interneurons. We conclude that motor neuron autophagy is required to maintain neuromuscular innervation early in disease but eventually acts in a non–cell-autonomous manner to promote disease progression.

amyotrophic lateral sclerosis | motor neuron | autophagy | non-cell autonomous

Amyotrophic lateral sclerosis (ALS) is a fatal neurodegenerative disease characterized by neuromuscular denervation, motor neuron death, and paralysis. Motor neurons that innervate fast-twitch muscle fibers are the first to degenerate, which leads to focal neurological deficits (1). This is followed by rapid disease progression, eventually leading to pathological changes in other motor neurons, interneurons, and glial cells. The preferential vulnerability of motor neurons and the mechanisms by which pathology spreads to other cell types during disease progression are poorly understood.

A hallmark of ALS pathology is the formation of ubiquitinated inclusion bodies in vulnerable cell types. Many ALS-causing genes encode aggregation-prone proteins, and disease-associated mutations can exacerbate inclusion formation (2, 3). Protein aggregation in ALS may be further propagated by prion-like template-directed misfolding (4). Another group of ALS-causing genes, including *p62*/*SQSTM1*, *OPTN*, *TBK1*, and *VCP*, converges on the macroautophagy pathway (5, 6). In particular, TBK1 lies at the interface of innate immunity and autophagy, as it binds to and phosphorylates multiple components of these pathways (7). Remarkably, although the pathological consequences of *C9ORF72* hexanucleotide repeat expansions have been well documented, recent studies have shown that the C9orf72 protein plays a role in macroautophagy as a part of a complex that is a phosphorylation target of TBK1 (8, 9). Taken together, the human genetic data suggest that the formation of ALS-associated protein aggregates is countered by macroautophagy and that mutations that adversely affect aggregate formation or removal can lead to ALS. Additionally, it is possible that aberrant or excessive activation of macroautophagy could contribute to neurodegeneration.

Macroautophagy, hereafter denoted as "autophagy," is a degradative mechanism in which a double-membrane autophagosome engulfs cytoplasmic substrates and subsequently fuses with the lysosome. Selective autophagy receptors such as p62 and OPTN bind specific substrates and guide them to nascent autophagosomes via their interaction with Atg8 homologs such as MAP1LC3 or GABARAP proteins (10). Although mutations in the autophagy pathway account for a small fraction of ALS cases, the ubiquitous accumulation of p62 in patient motor neurons suggests that dysregulation of this pathway may be a common feature of the disease (11).

In addition to participating in the removal of pathological protein aggregates, neuronal autophagy is also involved in cellular remodeling events. For example, inhibition of autophagy in dopaminergic neurons leads to striking changes in presynaptic structure and function (12, 13) and can affect developmental synaptic pruning in cortical neurons (14). Despite these intriguing results, the role of autophagy at the mammalian neuromuscular junction (NMJ) is not well understood.

Several studies have investigated the role of autophagy in transgenic mice expressing mutant forms of superoxide dismutase (SOD1)

Significance

Amyotrophic lateral sclerosis (ALS) is a neurodegenerative disease that leads to death of spinal motor neurons and paralysis. Genetic studies of ALS patients have identified mutations in autophagy pathway genes including *p62*/*SQSTM1*, *OPTN*, *TBK1*, *VCP*, and *C9ORF72*. However, the mechanisms by which these mutations cause ALS are not understood. Here we investigated the role of autophagy in a mouse model of ALS by specifically disrupting the critical autophagy gene *Atg7* in motor neurons. We found that inhibition of autophagy in motor neurons accelerated disease onset but prolonged lifespan. This increase in longevity was associated with a reduction in glial inflammation and interneuron pathology, indicating a non–cell-autonomous role for motor neuron autophagy in disease pathogenesis.

Author contributions: N.D.R., M.M.R., and T.M. designed research; N.D.R., C.J.G., V.G., X.W., and J.C.T. performed research; N.D.R., C.J.G., P.G., J.A.P., M.M.R., and T.M. analyzed data; and N.D.R. and T.M. wrote the paper.

Reviewers: V.L., University of Pennsylvania Perelman School of Medicine; and L.P., Mayo Clinic.

The authors declare no conflict of interest.

Data deposition: The data reported in this paper have been deposited in the Gene Expression Omnibus (GEO) database, https://www.ncbi.nlm.nih.gov/geo/query/acc.cgi?acc=GSE100888 (accession no. GSE100888).

[1]Present address: Department of Biomedical Sciences, University of Talca, 3460000 Talca, Chile.

[2]To whom correspondence should be addressed. Email: tm2472@columbia.edu.

This article contains supporting information online at www.pnas.org/lookup/suppl/doi:10.1073/pnas.1704294114/-/DCSupplemental.

that cause ALS in human patients. Autophagy induction by rapamycin was found to reduce lifespan, suggesting that autophagy may play a detrimental role in disease pathogenesis (15). Subsequent pharmacological and genetic studies have yielded conflicting results, but they are complicated by the nonspecific nature of the manipulations (16–22). To date, cell type-specific manipulation of the autophagy pathway in ALS mouse models has not been reported.

Here, we characterize autophagy abnormalities in the SOD1^{G93A} mouse model of ALS and find that the autophagy machinery is differentially recruited to ubiquitinated aggregates early and late in disease. Early in disease, vulnerable motor neurons form large autophagosomes containing ubiquitinated cargo recognized by the selective autophagy receptor p62. Other motor neurons and interneurons do not engulf cargo within autophagosomes and instead accumulate somatodendritic aggregates late in disease. Based on these results, we hypothesized that autophagy likely plays distinct roles early and late in disease progression. To test this hypothesis, we genetically suppressed autophagy in SOD1^{G93A} mice by conditionally disrupting the critical autophagy gene *Atg7* in motor neurons. We found that autophagy inhibition accelerated denervation of the vulnerable tibialis anterior muscle and the onset of hindlimb tremor in Atg7 conditional knockout (cKO); SOD1^{G93A} mice. Unexpectedly, however, autophagy inhibition also increased lifespan and decreased pathology in interneurons and glia. On the basis of these data, we propose that autophagy in motor neurons plays a protective role early in disease but eventually contributes to neurodegeneration in a non–cell-autonomous manner.

Results

Neuronal Subtype-Specific Aggregation of p62 in SOD1^{G93A} Spinal Cord. As a first step in understanding the role of autophagy in ALS, we characterized the autophagy pathway in the SOD1^{G93A} mouse model. Given the ubiquitous presence of p62 in ALS protein aggregates (11), we examined p62 pathology in the SOD1^{G93A} spinal cord. We identified motor neurons in the lumbar spinal cord using immunofluorescent labeling of choline acetyltransferase (ChAT). While WT motor neurons showed a diffuse cytoplasmic distribution of p62, a subset of SOD1^{G93A} motor neurons displayed p62 aggregates as early as postnatal day (P)50, well before symptom onset (Fig. 1*A*). High magnification revealed two distinct types of inclusions. In some SOD1^{G93A} motor neurons, p62 formed round bodies (RBs) measuring over 3 μm in diameter, whereas in others p62 formed skein-like inclusions (SLIs) that localized to the cell soma and dendrites (Fig. 1*B*). We quantified the abundance of these two types of aggregates over the course of disease progression. RBs were most abundant at P50 but became progressively less abundant with disease progression (6.17% of motor neurons at P50 vs. 0.56% at P150) (Fig. 1*C*). In contrast, SLIs were rare at the P50 time point but became more prevalent over the course of disease progression (0.85% of motor neurons at P50 vs. 10.05% at P150) (Fig. 1*C*). To avoid misinterpretation of these results due to motor neuron loss during disease progression, we also analyzed the absolute number of motor neurons with RBs and SLIs per ventral horn and found the same trends were present (Fig. S1*A*).

In addition to the time-dependent change in the prevalence of inclusion types, we also found that the different inclusion types segregated into distinct motor neuron populations. We found that motor neurons with RBs were the largest in the ventral horn, whereas motor neurons containing SLIs were similar in size to unaffected cells (Fig. S1*B*). The large size of RB-containing cells suggested that they might be fast motor neurons. Indeed, we found that they stained positive for matrix metalloproteinase-9 (MMP-9), a molecular marker for this vulnerable motor neuron subtype (Fig. 1*D* and Fig. S1*C*) (23). This observation suggests that RBs form specifically in fast motor neurons early in disease. In contrast, SLIs formed in motor neurons with lower MMP-9 expression and variable NeuN immunoreactivity (Fig. S1*D*), suggesting that they formed in slow alpha motor neurons as well as in smaller, NeuN-negative gamma motor neurons.

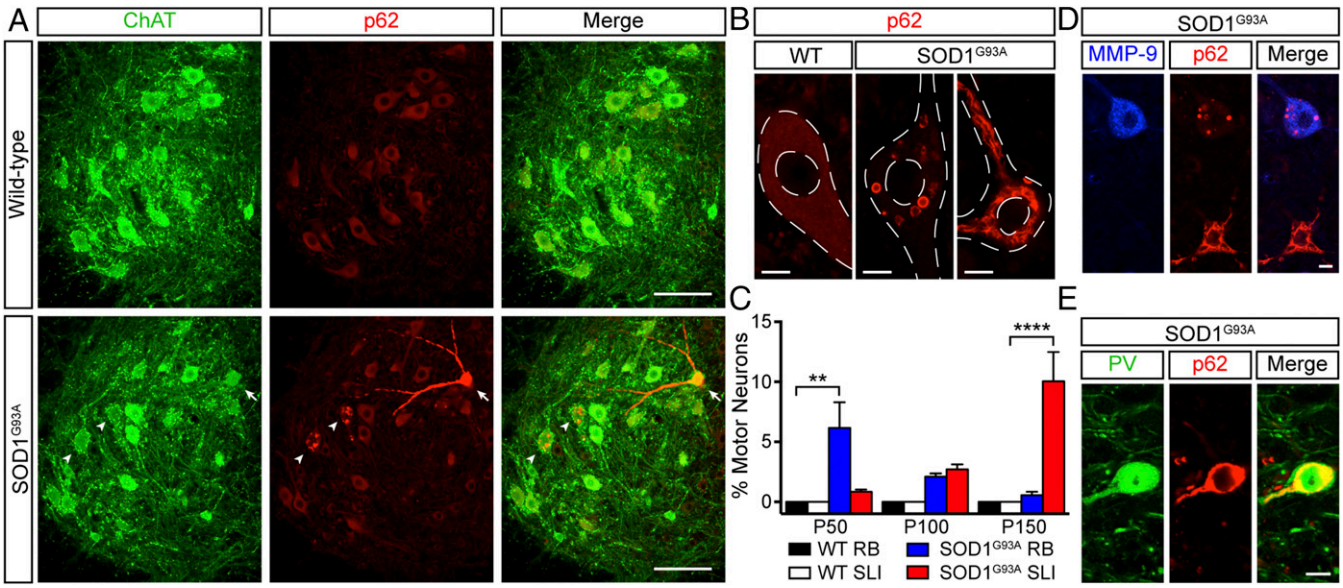

Fig. 1. Autophagy dysregulation in the SOD1^{G93A} mouse model. (*A*) Immunofluorescent labeling of ChAT (green) and p62 (red) reveals selective aggregation of p62 in P50 SOD1^{G93A} motor neurons. A subset of motor neurons shows p62 aggregation in RBs (arrowheads), while another subset shows p62 aggregation in SLIs (arrow). (Scale bars, 100 μm.) (*B*) High magnification of motor neurons shown in *A* stained for p62 (red). RB and SLI aggregates are depicted. (Scale bars, 10 μm.) (*C*) Quantification of motor neuron p62 aggregates reveals a decline in RB abundance and an increase in SLI abundance during disease progression. n = 3–4 animals per genotype. Data are shown as mean ± SEM; $^{**}P < 0.01$, $^{****}P < 0.0001$ (two-way ANOVA, Sidak's post hoc test). (*D*) Immunofluorescent labeling of p62 (red) and MMP-9 (blue) in a P100 SOD1^{G93A} mouse showing RB formation in an MMP-9–positive fast motor neuron (*Top*) but not an MMP-9–negative motor neuron (*Bottom*). (Scale bar, 10 μm.) (*E*) Immunofluorescent labeling of parvalbumin (green) and p62 (red) showing an SLI in an interneuron from a P150 SOD1^{G93A} mouse. (Scale bar, 10 μm.)

To determine whether p62 aggregation was specific to motor neurons, we asked whether p62 colocalized with additional cell-type markers. We did not observe colocalization of p62 with the astrocyte marker GFAP or the microglial marker Iba1 (Fig. S1 *E* and *F*). However, we did observe the formation of SLIs outside the ventral horn late in disease progression. We found that these cells stained positive for Nissl substance but negative for ChAT, indicating that they were interneurons (Fig. S1*G*). Their identity as interneurons was further confirmed by staining with the calcium-binding protein parvalbumin, which labeled a subset of the affected cells (Fig. 1*E*). Quantification of interneuron SLIs revealed a progressive accumulation that became especially prominent at the P150 time point (Fig. S1*H*). Thus, while SLIs first occurred in motor neurons, this marker of pathology eventually appeared in spinal interneurons.

Atg8 Homologs Surround RBs but Not SLIs. Autophagy receptors such as p62 link ubiquitinated proteins to Atg8 homologs via a ubiquitin-associated domain (UBA) and an LC3-interacting region (LIR) (24). Consistent with this role, p62-positive RBs and SLIs both stained positive for ubiquitin (Fig. 2*A*). While the full complement of ubiquitinated proteins in these inclusions remains unknown, we found that SOD1 selectively accumulated in SLIs but not in RBs (Fig. S2). The absence of SOD1 immunoreactivity in RBs may reflect limited antibody accessibility, or RBs may primarily contain other ubiquitinated cargo such as damaged mitochondria, as has been previously described (25).

We next asked whether p62 recruits Atg8 homologs to these ubiquitinated aggregates. We identified only weak LC3B immunoreactivity on the periphery of RBs (Fig. S3*A*). To circumvent limitations associated with antibody labeling, we bred SOD1^{G93A} mice to GFP-LC3 transgenic mice to visualize autophagosomes (26). Using this genetically encoded reporter, we found that RBs were surrounded by GFP-LC3, whereas this marker was largely absent in SLIs (Fig. S3*B*).

Despite the widespread use of LC3 as an autophagosome marker, other Atg8 homologs may be equally important. In particular, GABARAPL1 is expressed at high levels in spinal motor neurons (27, 28). We found that GABARAPL1 formed small, punctate structures in WT motor neurons (Fig. 2*B*). In SOD1^{G93A} motor neurons, GABARAPL1 robustly labeled p62-positive RBs, and this labeling was even more pronounced than LC3. Nonetheless, consistent with LC3 localization, GABARAPL1 was not observed surrounding SLIs (Fig. 2*B*). Based on the differential pattern of labeling with two different Atg8 homologs, we conclude that the RBs but not SLIs correspond to mature autophagosomes.

We hypothesized that the accumulation of ubiquitinated cargo without corresponding recruitment of the downstream autophagy machinery might lead to a cellular stress response. In particular, up-regulation of phosphorylated c-Jun (p-c-Jun) has been described in the nuclei of both motor neurons and interneurons containing ubiquitinated aggregates in SOD1^{G93A} mice (29). We found that nuclear p-c-Jun was specifically up-regulated in motor neurons with SLIs but rarely in motor neurons with RBs (Fig. 2 *C* and *D*). This observation suggests that failure to engulf cargo within GABARAPL1-positive autophagosomes is indeed associated with a neuronal stress response.

The recruitment of p62 to ubiquitinated aggregates might play a critical role in disease pathogenesis, or it may act cooperatively with other autophagy receptors. In support of the latter hypothesis, we found that the autophagy receptor NBR1 colocalized with p62 in RBs and SLIs (Fig. S4 *A* and *B*). Moreover, genetic deletion of p62 in SOD1^{G93A} mice did not block GABARAPL1 recruitment or p-c-Jun activation and failed to alter the disease phenotype (Fig. S4 *C*–*E*). Taken together, these results suggest that p62 is functionally redundant with other selective autophagy receptors.

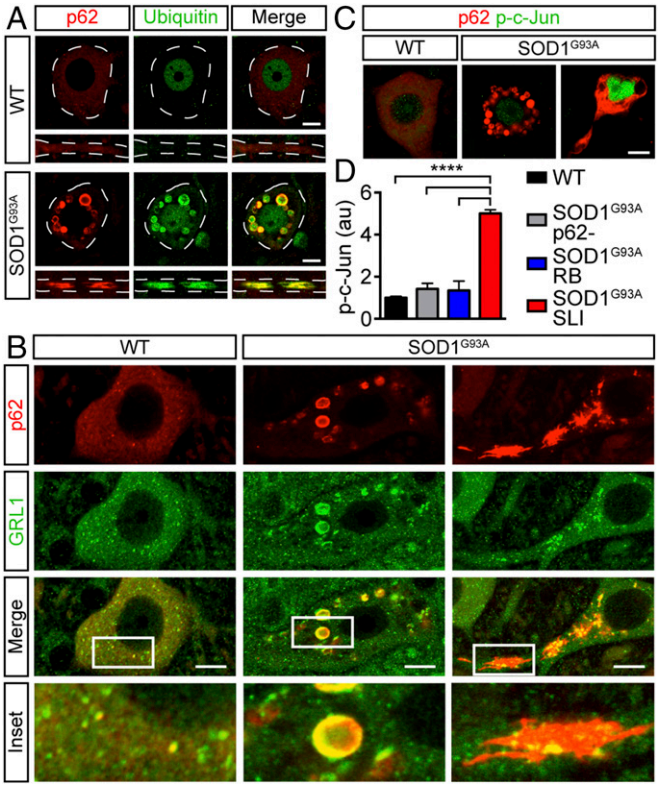

Fig. 2. Differential recruitment of GABARAPL1 to ubiquitinated RBs and SLIs. (*A*) Colocalization of ubiquitin (green) and p62 (red) in both RBs and SLIs in P50 SOD1^{G93A} mice. Motor neuron cell bodies and neurites are outlined in white. (Scale bars, 10 μm.) (*B*) Immunofluorescence labeling of p62 (red) and GABARAPL1 (GRL1, green) in P50 WT and SOD1^{G93A} motor neurons reveals complete colocalization for RBs but not SLIs. (Scale bars, 10 μm.) (*C*) Motor neurons with SLIs exhibit dramatic up-regulation of nuclear p-c-Jun (*Right*) that is not observed in SOD1^{G93A} motor neurons with RBs (*Middle*) or WT controls (*Left*). (Scale bar, 10 μm.) (*D*) Quantification of nuclear p-c-Jun intensity in WT motor neurons and SOD1^{G93A} motor neurons with RBs, SLIs, and those without p62 aggregates. Fluorescence intensity was normalized to the WT level and expressed as arbitrary units (au). $n = 3$ P100 animals per genotype. Data are shown as mean ± SEM; ****$P < 0.0001$ (one-way ANOVA, Tukey's post hoc test).

Autophagy Is Dispensable for Motor Neuron Survival but Regulates Synaptic Structure and Function. To better understand the role of autophagy in disease, we sought to achieve robust inhibition of autophagy in motor neurons. To do this, we used cKO mice for Atg7, an E1-like enzyme required for autophagosome biogenesis (30). We generated motor neuron-specific autophagy-deficient mice by crossing Atg7$^{flox/flox}$ mice to ChAT-Cre mice (Atg7 cKO) and compared them with littermate controls with intact Atg7 expression (Atg7 cWT). Autophagy deficiency in Atg7 cKO mice was confirmed by Western blot analysis of Atg5, LC3, and p62 (Fig. 3 *A* and *B*). Loss of Atg7 enzymatic activity led to the accumulation of monomeric Atg5 not conjugated to Atg12 and reduced the conversion of LC3 I to LC3 II. Autophagy deficiency also led to dramatic accumulation of p62, and immunofluorescence analysis confirmed that p62 predominantly accumulated within Atg7 cKO motor neuron cell bodies and neurites (Fig. 3*C* and Fig. S5*A*). As expected, recombination was also evident in a small population of cholinergic interneurons (Fig. S5*B*), but this was tolerated because they do not play an essential role in locomotion (31). At the ultrastructural level, large p62 bodies associated with motor neuron autophagy inhibition appeared as characteristic amorphous inclusions (Fig. S5*C*). To confirm that other degradative pathways remained intact, we measured proteasome abundance and activity

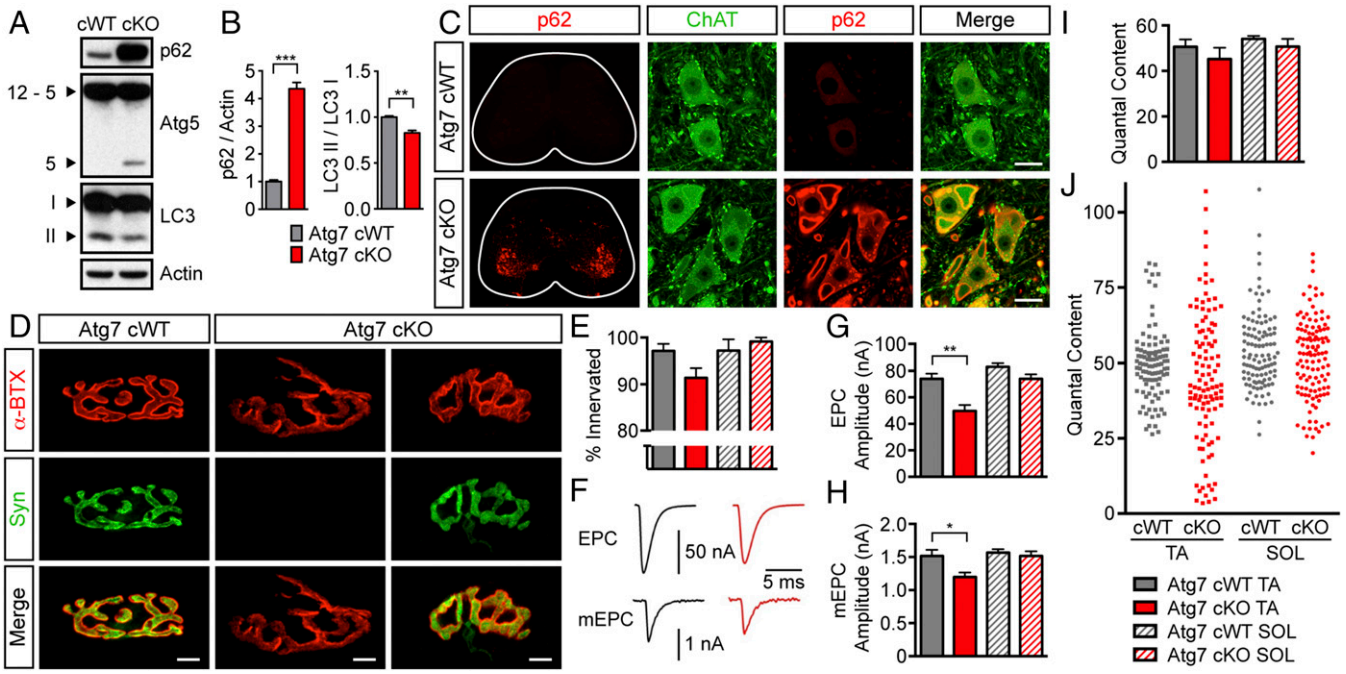

Fig. 3. Abnormal synaptic structure and function in Atg7 cKO mice. (*A*) Western blot analysis of lumbar spinal cord homogenates revealed increased p62 levels, the presence of monomeric Atg5, and a decrease in the LC3 II/I ratio in P150 Atg7 cKO mice. (*B*) Quantification of p62 levels normalized to actin and the LC3 II/I ratio. $n = 3$ animals per genotype. Data are shown as mean ± SEM; $^{**}P < 0.01$, $^{***}P < 0.001$ (two-tailed t test). (*C*) Immunofluorescent labeling of p62 (red) and ChAT (green) in P150 Atg7 cKO mice and Atg7 cWT controls. The outline of a whole spinal cord segment is shown in the low-magnification panels on the left. (Scale bar, 25 μm.) (*D*) Motor endplates labeled with α-bungarotoxin (red) and synaptophysin-positive presynaptic terminals (green) from the tibialis anterior muscles of P150 Atg7 cWT and Atg7 cKO mice. (Scale bars, 8 μm.) (*E*) Quantification of NMJs revealed no significant difference in the innervation of the tibialis anterior (TA) or soleus (SOL) from P150 Atg7 cKO mice compared with Atg7 cWT controls. $n = 3$–4 animals per genotype. Data are shown as mean ± SEM; $P = 0.0694$ (one-way ANOVA). (*F*) EPC (*Upper*) and mEPC (*Lower*) traces from tibialis anterior NMJs in P100 Atg7 cWT (black traces) and Atg7 cKO (red traces) mice. Each trace is an average of six EPCs or >30 mEPCs recorded from a single NMJ. (*G* and *H*) Amplitudes of EPCs (*G*) and mEPCs (*H*) were selectively reduced at Atg7 cKO tibialis anterior NMJs but not at soleus NMJs compared with Atg7 cWT controls. $n = 5$–6 animals per genotype (>6 NMJs per animal). Data are shown as mean ± SEM; $^{*}P < 0.05$, $^{**}P < 0.01$ (one-way ANOVA, Tukey's post hoc test). (*I*) Quantal content did not differ significantly between muscles from different genotypes. $n = 5$–6 animals per genotype. Data are shown as mean ± SEM; $P = 0.3533$ (one-way ANOVA). (*J*) The distribution of quantal content measurements from individual NMJs revealed a population of low-quantal-content synapses in the Atg7 cKO tibialis anterior (red squares) that was not observed in the Atg7 cWT tibialis anterior (gray squares), Atg7 cKO soleus (red circles), or Atg7 cWT soleus (gray circles). $n = 109$, 99, 118, and 108 NMJs, respectively.

in Atg7 cWT and Atg7 cKO spinal cord lysates and found no significant differences (Fig. S5 *D*–*F*).

Before breeding Atg7 cKO mice to the SOD1^{G93A} mouse model, we asked whether inhibition of motor neuron autophagy alone was sufficient to cause neurodegeneration. Consistent with a previous report, Atg7 cKO mice were viable and did not display overt neurological defects (32). We quantified the number of ChAT-positive motor neurons in the L4–L5 spinal segments and found no effect of autophagy inhibition (Fig. S5*G*). Morphometric analysis revealed that Atg7 cKO motor neurons were 37% larger than in Atg7 cWT controls, although the normal bimodal size distribution of the motor neurons was maintained (Fig. S5 *H* and *I*). We conclude that autophagy in motor neurons is dispensable for cell survival but negatively regulates cell size.

Neuronal autophagy may play a specialized role in the regulation of axonal and synaptic morphology. To determine the effect of autophagy inhibition on motor neuron presynaptic terminals, we investigated NMJs in Atg7 cKO mice. We began by visualizing the innervation of synaptophysin-positive presynaptic terminals onto α-bungarotoxin–positive postsynaptic acetylcholine receptors in the tibialis anterior muscle. Consistent with intact motor function in Atg7 cKO mice, we found that the vast majority of NMJs maintained normal innervation (Fig. 3 *D* and *E*). However, some denervated endplates were observed (Fig. 3*D*), and there was an overall trend toward denervation relative to Atg7 cWT controls (Fig. 3*E*). We confirmed neuromuscular denervation of the tibialis anterior using electron microscopy. In control mice we observed normal apposition of the presynaptic terminal and motor endplate. While intact NMJs were also observed in Atg7 cKO mice, some NMJs exhibited postsynaptic folds with no presynaptic axon terminal apposed to them (Fig. S5*J*).

In contrast to the tibialis anterior muscle, which is primarily composed of fast-twitch muscle fibers that are denervated early in SOD1^{G93A} disease progression, the soleus is composed of slow-twitch fibers that maintain innervation until late stages of disease (33). We investigated neuromuscular innervation in the soleus and found no evidence of endplate denervation (Fig. 3*E*), suggesting that autophagy inhibition selectively compromised the integrity of NMJs known to be vulnerable in ALS.

To investigate whether neurotransmission was altered by autophagy inhibition, we recorded electrophysiological activity at NMJs. We found that endplate current (EPC) amplitude evoked by nerve stimulation was markedly decreased at tibialis anterior NMJs in Atg7 cKO mice, but similar defects were not observed at soleus NMJs (Fig. 3 *F* and *G*). A single EPC reflects the simultaneous release of many synaptic vesicles, while a miniature endplate current (mEPC) reflects a single vesicle-release event. We found that mEPC amplitude was reduced at tibialis anterior NMJs, suggesting that this was a major contributor to reduced EPC amplitude in mutant mice (Fig. 3*H*). In addition, the number of synaptic vesicles released (the quantal content) was severely reduced at a subset of tibialis anterior NMJs (Fig. 3 *I* and *J*). Thus, defects in both mEPC amplitude and quantal content contributed to reduced EPC amplitude in Atg7 cKO mice, and both these parameters were selectively

impaired at tibialis anterior but not soleus NMJs. In contrast, other aspects of synaptic transmission, such as increased fatigue upon repetitive stimulation, were impaired in both muscles (Fig. S5 *K* and *L*). These data suggest that autophagy inhibition in motor neurons results in multiple abnormalities in neurotransmission that are particularly severe at tibialis anterior NMJs.

Inhibition of Motor Neuron Autophagy Accelerates Disease Onset but Extends Lifespan in SOD1^{G93A} Mice. To investigate the involvement of motor neuron autophagy in ALS disease pathogenesis, we bred Atg7 cKO mice to SOD1^{G93A} mice to generate Atg7 cKO; SOD1^{G93A} double-mutant mice. We hypothesized that structural and functional defects at motor neuron presynaptic terminals might exacerbate neuromuscular denervation in SOD1^{G93A} mice. However, temporal changes in p62 aggregation and the recruitment of Atg8 homologs suggested that the role of autophagy, and therefore the effects of autophagy inhibition, could vary during the course of disease progression.

To measure disease onset in Atg7 cKO; SOD1^{G93A} mice, we monitored mice for the onset of hindlimb tremor and the onset of disease-associated weight loss. We found that Atg7 cKO; SOD1^{G93A} mice exhibited accelerated onset of hindlimb tremor compared with Atg7 cWT; SOD1^{G93A} controls (median age of onset: 78 d versus 100 d) (Fig. 4*A*). Although this metric of disease onset was robustly accelerated, we did not find any difference in the onset of disease-associated weight loss between Atg7 cKO; SOD1^{G93A} mice and Atg7 WT; SOD1^{G93A} controls (median age of onset: 105 d versus 98 d) (Fig. 4*B*). These data indicate that the two metrics of disease onset can be uncoupled and that motor neuron autophagy inhibition specifically accelerates early signs of neurological dysfunction.

We measured lifespan by determining the age at which disease-associated paralysis prevented a mouse from righting itself after being placed on its side. Surprisingly, we found a dramatic 21.7% extension of lifespan in Atg7 cKO; SOD1^{G93A} mice compared with Atg7 cWT; SOD1^{G93A} controls (median age of disease end stage: 185 d versus 152 d) (Fig. 4*C*). Thus, despite the fact that motor neuron autophagy inhibition accelerated disease onset, this manipulation eventually delayed the later stages of SOD1^{G93A} disease progression.

We next asked whether changes in symptom onset and lifespan could be explained by changes in motor neuron survival. We quantified the number of ChAT-positive motor neurons in the L4–L5 lumbar segments across the course of disease progression. As expected, Atg7 cWT; SOD1^{G93A} mice exhibited gradual degeneration of motor neurons that became significant at P150. However, in contrast to the striking phenotypic changes observed upon motor neuron autophagy inhibition, we did not find any significant differences in motor neuron survival in Atg7 cKO; SOD1^{G93A} mice (Fig. S6 *A* and *B*). These data indicate that the effect of motor neuron autophagy inhibition on lifespan is not due to enhanced motor neuron survival. We also examined whether the distribution of SOD1 was altered in Atg7 cKO; SOD1^{G93A} motor neurons. While it appeared to be excluded from large p62 bodies associated with autophagy inhibition, the distribution was otherwise similar to that observed in Atg7 cWT; SOD1^{G93A} mice (Fig. S6*C*).

NMJ degeneration precedes motor neuron loss in SOD1^{G93A} mice and therefore serves as a highly sensitive anatomical correlate of disease. As expected, we observed progressive denervation of the fast tibialis anterior muscle during the course of disease

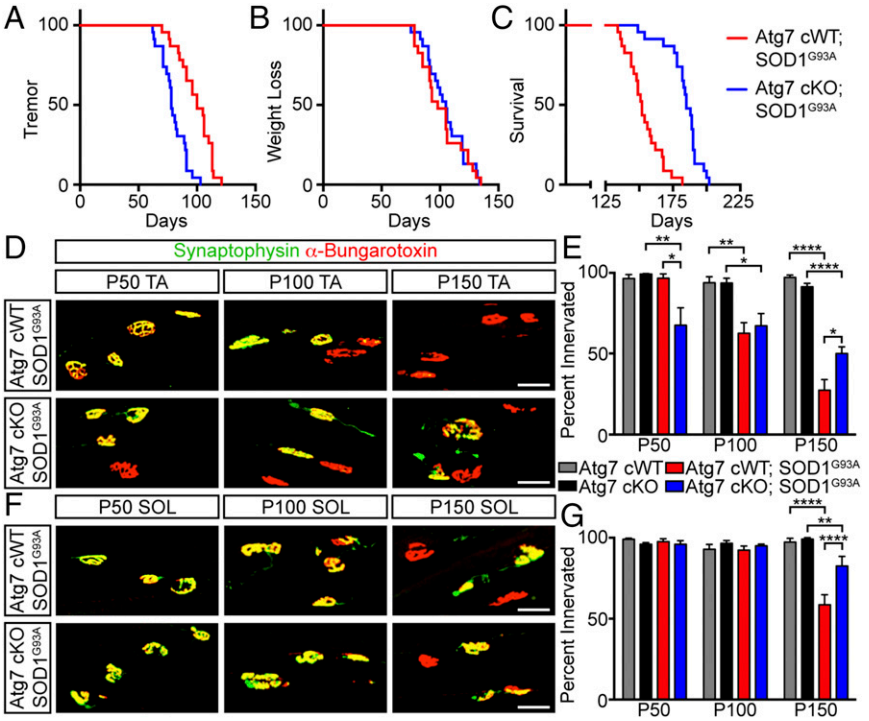

Fig. 4. Inhibition of autophagy in motor neurons accelerates early SOD1^{G93A} disease pathology but extends lifespan. (*A*–*C*) Kaplan–Meier plots showing effects of motor neuron autophagy inhibition on disease phenotypes. (*A*) Onset of tremor is accelerated by 22.0% in Atg7 cKO; SOD1^{G93A} mice relative to Atg7 cWT; SOD1^{G93A} controls. Log-rank test = 21.49; $P < 0.0001$. (*B*) Genotype had no effect on the onset of weight loss. Log-rank test = 0.1039; $P = 0.7472$. (*C*) Lifespan is extended by 21.7% in Atg7 cKO; SOD1^{G93A} mice relative to Atg7 cWT; SOD1^{G93A} controls. Log-rank test = 38.03; $P < 0.0001$. $n = 23$ animals per genotype. (*D*) Tibialis anterior NMJs revealed by presynaptic synaptophysin (green) and postsynaptic α-bungarotoxin (red) labeling. (Scale bars, 50 μm.) (*E*) Autophagy inhibition increases denervation of the tibialis anterior at P50 but preserves synaptic innervation at P150. $n = 3$–5 animals per genotype per time point. Data are shown as mean ± SEM; $^*P < 0.05$, $^{**}P < 0.01$, $^{****}P < 0.0001$ (two-way ANOVA, Tukey's post hoc test). (*F*) Soleus NMJs revealed by presynaptic synaptophysin (green) and postsynaptic α-bungarotoxin (red) labeling. (Scale bars, 50 μm.) (*G*) Autophagy inhibition reduces denervation of the soleus at P150. $n = 3$–5 animals per genotype per time point. Data are shown as mean ± SEM; $^{**}P < 0.01$, $^{****}P < 0.0001$ (two-way ANOVA, Tukey's post hoc test).

progression in Atg7 cWT; SOD1^{G93A} controls. However, autophagy inhibition in motor neurons altered the course of denervation. Initial denervation was markedly accelerated in Atg7 cKO; SOD1^{G93A} mice. Nonetheless, by P150 they retained a higher percentage of innervated NMJs than their Atg7 cWT; SOD1^{G93A} counterparts (Fig. 4 *D* and *E*). Thus, loss of autophagy in motor neurons accelerated early denervation of the tibialis anterior but eventually preserved NMJ innervation late in disease. This may reflect slowing of denervation late in disease, increased reinnervation, or a combination of both these processes (34).

We next extended our analysis of neuromuscular innervation to the soleus muscle. Consistent with the relative resistance of the soleus in motor neuron disease, we did not detect denervation in any genotype until P150. At this time point, Atg7 cWT; SOD1^{G93A} mice showed significant denervation that was attenuated in Atg7 cKO; SOD1^{G93A} mice (Fig. 4 *F* and *G*). Thus, in contrast to the tibialis anterior, motor neuron autophagy inhibition had no effect on neuromuscular innervation of the soleus early in disease. However, as in the tibialis anterior, loss of motor neuron autophagy preserved neuromuscular innervation late in disease.

Non–Cell-Autonomous Effect of Motor Neuron Autophagy on Glia and Interneuron Pathology. The expression of mutant SOD1 causes early motor neuron degeneration through cell-autonomous mechanisms, whereas further disease progression is mediated largely by other cell types such as astrocytes and microglia (35, 36). We therefore investigated whether the loss of autophagy in motor neurons influenced glial reactivity late in disease progression. To measure astrogliosis, we quantified GFAP immunoreactivity in the ventral horn, intermediate zone, and dorsal horn. We observed dramatic up-regulation of GFAP along the entire dorsal–ventral axis of the spinal cord in Atg7 cWT; SOD1^{G93A} mice compared with Atg7 cWT controls. In contrast, we found a global reduction of this marker in spinal cord sections from P150 Atg7 cKO; SOD1^{G93A} mice (Fig. 5 *A* and *B*). Immunostaining microglia with an antibody against Iba1 revealed a similar effect of motor neuron autophagy inhibition. Microglial activation was barely detectable in the P150 Atg7 cKO; SOD1^{G93A} spinal cord (Fig. 5 *C* and *D*). Thus, microglia may be more directly affected by the loss of autophagy in motor neurons, whereas altered astrogliosis could be secondary to changes in microglial activation.

Finally, we examined spinal interneurons, which develop SLI pathology late in disease progression (Fig. S1*H*). Strikingly, SLIs were virtually absent from spinal interneurons in Atg7 cKO; SOD1^{G93A} mice at P150 (Fig. 5*E*). We quantified the percent of Nissl-positive, ChAT-negative interneurons with SLI pathology and found a significant reduction in Atg7 cKO; SOD1^{G93A} mice relative to Atg7 cWT; SOD1^{G93A} controls (Fig. 5*F*). In contrast, loss of autophagy had no effect on the percentage of motor neurons with SLIs (Fig. 5*F*). Interneuron pathology and glial activation did eventually become evident in end-stage Atg7 cKO; SOD1^{G93A} mice (Fig. S7), suggesting that these processes were delayed, but not completely blocked, by motor neuron autophagy inhibition.

We hypothesized that the delay in interneuron SLI formation might lead to a corresponding reduction in SOD1 aggregation. Similar to motor neurons, we found that misfolded SOD1 colocalized with p62 in interneuron SLIs (Fig. S8*A*). Furthermore, the previously reported (37) biochemical interaction between p62 and mutant SOD1 was strongest at disease end stage, when SLI pathology is most abundant (Fig. S8*B*). Consistent with reduced interneuron pathology in Atg7 cKO; SOD1^{G93A} spinal cords relative to Atg7 cWT; SOD1^{G93A} controls, the interaction between p62 and SOD1 was dramatically reduced by autophagy inhibition (Fig. S8 *C* and *D*). Importantly, this reduction in binding was accompanied by a twofold reduction in the amount of insoluble SOD1 (Fig. S8 *E* and *F*).

The reduction in SLI pathology was also associated with dramatically reduced p-c-Jun immunoreactivity in the nuclei of spinal interneurons (Fig. 5*E*, *Inset*), which was also evident from Western blotting of spinal cord lysates (Fig. 5*G*). Quantification confirmed the presence of increased p-c-Jun in lysates from Atg7 cWT; SOD1^{G93A} mice but not Atg7 cKO; SOD1^{G93A} mice (Fig. 5*H*). Thus, autophagy inhibition in motor neurons led to a non–cell-autonomous reduction in p62 aggregation and p-c-Jun up-regulation in spinal interneurons.

Inhibition of Motor Neuron Autophagy Mitigates Disease-Associated Transcriptional Signature. The expression of mutant SOD1 leads to complex transcriptional changes in motor neurons and other spinal cord cell types (38). We reasoned that reduced glia and interneuron pathology in Atg7 cKO; SOD1^{G93A} mice would attenuate these pathological changes in gene expression. To test this hypothesis, we sequenced RNA from P150 lumbar spinal cords and analyzed gene expression. Hierarchical clustering of the RNA-sequencing (RNA-seq) data revealed that the loss of motor neuron autophagy had very little influence on gene expression in the absence of disease (Fig. S9*A*). However, in the context of mutant SOD1 expression, motor neuron autophagy inhibition caused many genes to be differentially expressed (Fig. S9*B*). Using gene set enrichment analysis (GSEA), we identified pathways involved in innate immunity and cytokine signaling as the pathways most differentially enriched in Atg7 cWT; SOD1^{G93A} mice relative to Atg7 cKO; SOD1^{G93A} mice (Fig. S9*C*). In contrast, pathways involved in neuronal function and synaptic transmission were the pathways most differentially enriched in Atg7 cKO; SOD1^{G93A} mice relative to Atg7 cWT; SOD1^{G93A} mice (Fig. S9*C*).

To specifically address the transcriptional activity of c-Jun, we analyzed a group of experimentally validated neuronal c-Jun target genes (39). We observed specific up-regulation of these genes in Atg7 cWT; SOD1^{G93A} spinal cords that was not observed in Atg7 cKO; SOD1^{G93A} spinal cords (Fig. 6*A*). Thus, the reduction in SLI pathology in spinal interneurons leads to a corresponding decrease in the transcription of neuronal c-Jun target genes.

Finally, we analyzed our RNA-seq data to address changes in the cellularity of the spinal cord in different genotypes. To do this, we used cell type-specific transcriptional signatures identified by previous studies (38, 40–43). We found selective enrichment of astrocyte and microglial markers in Atg7 cWT; SOD1^{G93A} mice that was not observed in Atg7 cKO; SOD1^{G93A} mice. We also found that motor neuron markers were depleted in SOD1^{G93A} mice regardless of autophagy inhibition. This is in contrast to general neuronal markers, which were specifically depleted in Atg7 cWT; SOD1^{G93A} mice but were relatively preserved in Atg7 cKO; SOD1^{G93A} mice (Fig. 6*B*). Thus, the transcriptional data are consistent with our histological findings: Autophagy inhibition had little effect on motor neuron abundance but led to non–cell-autonomous effects on other neuronal subtypes and glial cells.

Discussion

Here we show that autophagy in motor neurons plays counteracting roles early and late in disease progression in the SOD1^{G93A} mouse model of ALS. Early in disease progression, vulnerable motor neurons form large GABARAPL1-positive autophagosomes containing ubiquitinated cargo recognized by p62. Inhibition of motor neuron autophagy in SOD1^{G93A} mice accelerates the denervation of fast muscle fibers and the onset of tremor, indicating that autophagy plays a beneficial role early in disease. Late in disease, p62 aggregates are not engulfed by autophagy machinery, and this is associated with up-regulation of p-c-Jun in interneurons and widespread glial activation. Inhibition of motor neuron autophagy attenuates these pathological changes and extends lifespan, indicating that autophagy plays a detrimental role late in disease.

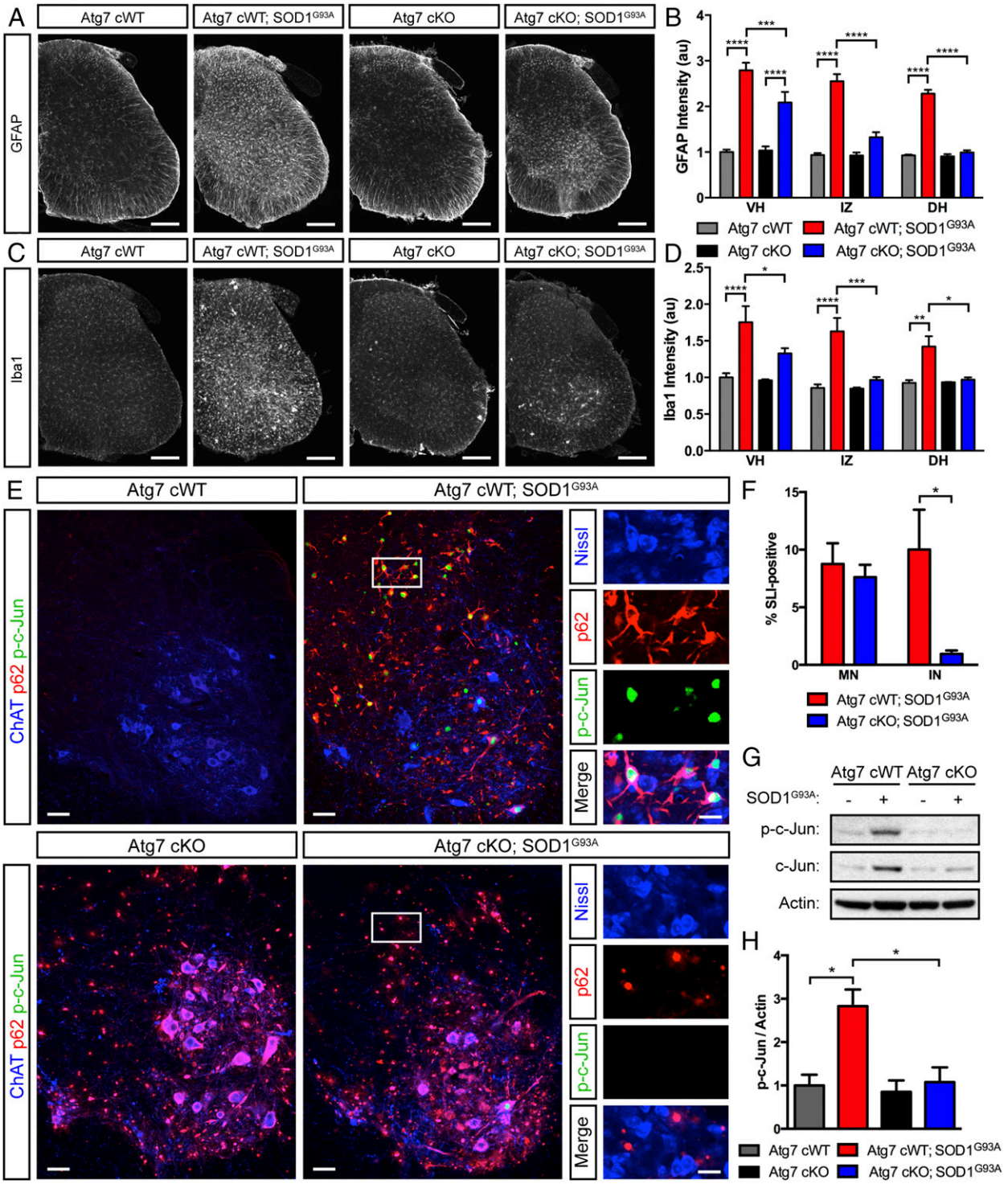

Fig. 5. Non–cell-autonomous effect of motor neuron autophagy inhibition on glial and interneuron pathology. (*A*) Immunofluorescent labeling of GFAP in lumbar spinal cord sections from the indicated genotypes at P150. (Scale bars, 200 μm.) (*B*) Quantification of GFAP intensity in the ventral horn (VH), intermediate zone (IZ), and dorsal horn (DH) of the spinal cord in arbitrary units (au). $n = 3$ animals per genotype. Data are shown as mean ± SEM; $^{***}P < 0.001$, $^{****}P < 0.0001$ (two-way ANOVA, Tukey's post hoc test). (*C*) Immunofluorescent labeling of Iba1 in lumbar spinal cord sections from the indicated genotypes at P150. (Scale bars, 200 μm.) (*D*) Quantification of Iba1 intensity in the ventral horn, intermediate zone, and dorsal horn in arbitrary units. $n = 3$ animals per genotype. Data are shown as mean ± SEM; $^{*}P < 0.05$, $^{**}P < 0.01$, $^{***}P < 0.001$, $^{****}P < 0.0001$ (two-way ANOVA, Tukey's post hoc test). (*E*) Immunofluorescence labeling of ChAT (blue), p62 (red), and p-c-Jun (green) in spinal cords from P150 mice. (Scale bars, 50 μm.) (*Insets*) High magnification of the boxed regions of interest shows immunofluorescence labeling of Nissl-positive interneurons (blue), p62 (red), and p-c-Jun (green). (Scale bars, 20 μm.) (*F*) Quantification of Nissl-positive, ChAT-negative interneurons (IN) reveals a lower frequency of SLI pathology in P150 Atg7 cKO; SOD1^{G93A} mice than in Atg7 cWT; SOD1^{G93A} controls. The frequency of SLI pathology in motor neurons (MN) does not differ between genotypes. $n = 3$ animals per genotype. Data are shown as mean ± SEM; $^{*}P < 0.05$ (two-way ANOVA, Sidak's post hoc test). (*G*) Western blot analysis of P150 lumbar spinal cord lysates reveals elevated levels of p-c-Jun and c-Jun only in Atg7 cWT; SOD1^{G93A} mice. (*H*) Quantification of p-c-Jun levels normalized to actin. $n = 3$ animals per genotype. Data are shown as mean ± SEM; $^{*}P < 0.05$ (one-way ANOVA, Tukey's post hoc test).

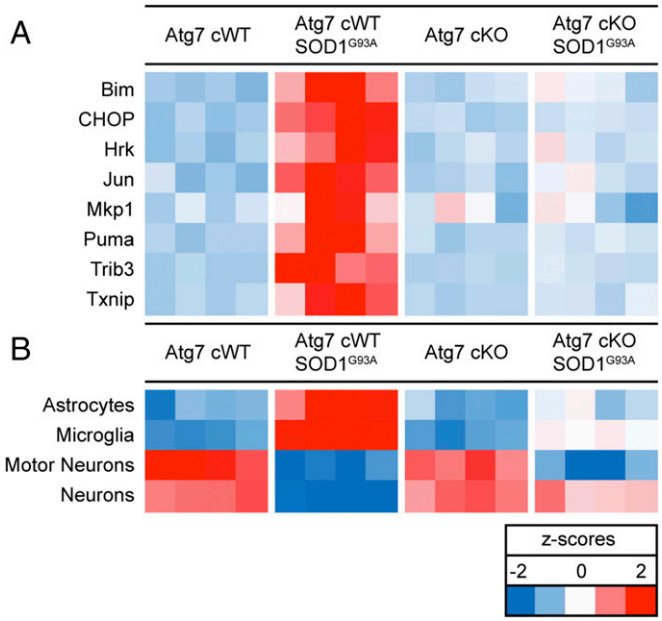

Fig. 6. Inhibition of motor neuron autophagy attenuates the SOD1^{G93A} transcriptional signature. (*A*) Heatmap showing relative expression level of neuronal c-Jun target genes in the indicated genotypes. Subcolumns represent biological replicates. (*B*) Heatmap of normalized enrichment scores for cell type-specific transcriptional signatures. Subcolumns represent biological replicates.

Neuronal Subtype-Specific Dependence on Autophagy. Most ALS-causing mutations are found in genes that are ubiquitously expressed, but motor neurons are especially vulnerable to these genetic insults. Even among these cells, fast motor neurons degenerate early, whereas other motor neurons do not degenerate until late in disease (1). Understanding the cellular properties that confer vulnerability to some motor neurons and resilience to others could help identify novel therapeutic strategies.

Our results reveal unexpected diversity in the regulation of neuronal autophagy in disease. Several lines of evidence suggest that the most vulnerable fast motor neurons are also the most dependent on autophagy. First, recruitment of Atg8 homologs to pathological protein aggregates recognized by p62 selectively occurs in the largest, MMP-9–positive motor neurons. Second, inhibition of autophagy through targeted disruption of *Atg7* leads to structural and functional defects at a subset of tibialis anterior NMJs without causing similar defects at soleus NMJs. Third, breeding these mice to the SOD1^{G93A} mouse model leads to accelerated denervation of the tibialis anterior early in disease, whereas autophagy inhibition does not similarly accelerate denervation of the soleus. In contrast, the only effect of autophagy inhibition in the soleus was to maintain neuromuscular innervation late in disease.

We found that loss of autophagy also accelerated the onset of hindlimb tremor in Atg7 cKO; SOD1^{G93A} mice. Tremor in this mouse model likely reflects dysfunction in the motor neuron–Renshaw cell circuit, which is involved in the suppression of tremor through feedback inhibition (44, 45). Fast motor neurons activate Renshaw cells to a much greater extent than slow motor neurons (46), suggesting that acceleration of tremor reflects specific dysfunction in fast motor units in Atg7 cKO; SOD1^{G93A} mice. However, we cannot rule out the possibility that autophagy inhibition in ChAT-positive cells other than motor neurons could also contribute to the earlier onset of tremor in these mice.

The dependence of fast motor neurons on autophagy may be one of the factors that render them more vulnerable in disease. SOD1^{G93A} motor neurons progressively lose lysosomal function during disease progression (25). Because fast motor neurons are especially dependent on autophagy, downstream defects in autophagic flux may preferentially affect these cells. In contrast, because autophagy machinery is not recruited to ubiquitinated aggregates in other motor neurons and interneurons, they may be more tolerant of lysosomal dysfunction. Nonetheless, unopposed somatodendritic accumulation of ubiquitinated proteins may eventually harm these cells through independent mechanisms, leading to the up-regulation of p-c-Jun and an inflammatory response.

Autophagy Regulates NMJ Structure and Function. Our findings support a role for neuronal autophagy in the regulation of presynaptic terminals. Despite the dramatic accumulation of p62-positive inclusions in Atg7 cKO motor neurons, we did not detect overt cell death. However, abnormalities in presynaptic structure were readily observed by light and electron microscopy. These changes were also accompanied by altered neurotransmission. Some of these electrophysiological abnormalities, such as decreased quantal content at a subset of tibialis anterior NMJs, clearly reflect defects in presynaptic function. A role for autophagy at the synapse was also apparent upon crossing Atg7 cKO mice to the SOD1^{G93A} mouse model. Even in presence of mutant SOD1 expression, autophagy inhibition selectively modulated neuromuscular denervation without affecting the rate of motor neuron cell death.

A presynaptic role for autophagy is also consistent with previous studies. In both Purkinje and midbrain dopaminergic neurons the loss of Atg7 leads to degenerative changes at presynaptic terminals (12, 13, 47). These studies clearly demonstrate a role for autophagy at the synapse, but generally only a subset of synapses is affected. While it is possible that the effects of autophagy inhibition are simply stochastic, the incomplete penetrance of these phenotypes may also reflect latent neuronal heterogeneity. This scenario is consistent with our finding that motor neuron subtypes are differentially dependent on autophagy for maintaining neuromuscular innervation.

The mechanism by which autophagy regulates presynaptic structure and function remains unclear. It has been demonstrated that autophagosomes can form distally at the synapse and retrogradely transport cargo for degradation (48). Thus, autophagy may be directly involved in recycling synaptic contents. Alternatively, it may influence synaptic innervation indirectly, perhaps via a signaling intermediate. For example, autophagy promotes neuromuscular innervation in *Drosophila* through the down-regulation of Highwire, an E3 ubiquitin ligase that negatively regulates NMJ growth (49). Mammalian motor neurons may use similar mechanisms, or it is possible that autophagic turnover of other substrates such as mitochondria is required for maintaining metabolically demanding structures such as long axons. Future studies can elucidate the specific cargos that are degraded by autophagy in motor neurons and how these substrates may change during the course of disease.

Late in disease, we find that autophagy inhibition in motor neurons helps preserve neuromuscular innervation. This effect occurs at a time point when the most vulnerable fast motor neurons have already degenerated (23), suggesting that other motor neuron subtypes may benefit from loss of autophagy. This protection could be partially cell autonomous, as neuronal autophagy may participate in some forms of synaptic pruning (14). However, our data strongly support a non–cell-autonomous component in the improved phenotype of Atg7 cKO; SOD1^{G93A} mice.

Loss of Motor Neuron Autophagy Delays Interneuron and Glial Pathology. A defining feature of human ALS is the relentless progression of motor dysfunction. Although the initial site of symptom onset is focal, symptoms quickly spread in a manner reflective of the underlying organization of neuronal circuitry (50, 51). Elucidating the cellular processes involved in disease spread could have profound therapeutic value for patients in the early stages of the disease.

We find that p62 aggregates in motor neurons temporally precede SLI pathology in spinal interneurons. This is consistent with previous reports of interneuron degeneration in ALS patients and

mouse models (52–54). Interneuron pathology was associated with up-regulation of p-c-Jun, a transcription factor that is aberrantly activated in ALS patients and may contribute to neurodegeneration by promoting the transcription of proapoptotic factors (39, 55). Aggregation of p62 and p-c-Jun up-regulation in interneurons occurs in tandem with astrogliosis and microgliosis, suggesting that these may be interrelated processes that contribute to the development of paralysis late in disease. From our results, we cannot determine whether the progression of pathology from motor neurons to interneurons is mediated by the direct spread of misfolded proteins. An alternative explanation is that these cell types simply have different intrinsic thresholds for aggregation. Nonetheless, our results do indicate that motor neuron autophagy has a non–cell-autonomous influence on the formation of protein aggregates in interneurons and glial inflammation.

Unexpectedly, activation of astrocytes and microglia was suppressed in Atg7 cKO; $SOD1^{G93A}$ mice, and the formation of p62 aggregates in interneurons was greatly reduced. This was accompanied by decreased transcription of genes involved in innate immunity, cytokine signaling, and the p-c-Jun transcriptional stress response. Although early transcriptional changes in mice expressing mutant SOD1 may be due to pathological changes within motor neurons, the neuroinflammatory signature at disease end stage is thought to be due to secondary RNA dysregulation in other cell types (56). Therefore, the reduced activation of these pathways in Atg7 cKO; $SOD1^{G93A}$ mice likely reflects a failure of autophagy-deficient motor neurons to trigger pathological changes in neighboring glia and interneurons.

Our results suggest that motor neuron autophagy promotes the progression of ALS-associated pathology in other cell types. This is consistent with accumulating evidence suggesting a role for autophagy in the spread of neurodegeneration. In a mouse model of Alzheimer's disease, loss of Atg7 dramatically reduced the amount of extracellular Aβ (57). In Parkinson's disease, autophagy has been implicated in the unconventional secretion of α-synuclein (58). This is consistent with accumulating evidence that autophagy and exosome release are coupled (59) and that aggregated proteins may be released from cells through exosomes (60). Thus, future work must examine whether similar autophagy-dependent secretory pathways are involved in ALS pathogenesis.

Our results build on previous studies of autophagy in mice expressing mutant SOD1. Rapamycin administration activated autophagy and exacerbated disease, whereas haploinsufficiency for Beclin-1 inhibited autophagy and extended survival (15, 19). Despite demonstrating a detrimental role for autophagy, these phenotypes likely reflect the composite effects of manipulating many different cell types. We extend these findings by showing that inhibition of autophagy specifically in motor neurons is sufficient to prolong lifespan. Our targeted manipulation also revealed a striking non–cell-autonomous role for motor neuron autophagy in the progression of disease pathology. By applying a similar approach to other spinal cord cell types, we will be able to further refine our understanding of autophagy in ALS pathogenesis.

Promoting the degradation of protein aggregates by autophagy is an attractive strategy in the treatment of neurodegenerative disease, but our study implies that great care must be taken in targeting this pathway. We show that inhibiting autophagy can have radically different effects early and late in disease progression. Any therapeutic approaches must take into account these highly context-dependent effects.

Materials and Methods

Animals. All mouse experimental procedures were approved by the Columbia University Medical Center Institutional Animal Care and Use Committee. All survival studies were performed with $SOD1^{G93A}$ transgenic mice on a C57/Bl6 genetic background. Mice were monitored for weight, tremor, and righting reflex to determine disease onset and lifespan (details are given in *SI Materials and Methods*).

Immunohistochemistry. All mouse tissue was fixed in 4% paraformaldehyde (PFA). Muscles were embedded and frozen at −80 °C before cryosectioning. Lumbar spinal cords were processed using a vibratome to generate free-floating sections. Tissue samples were blocked before incubating with primary and secondary antibodies (details are given in *SI Materials and Methods*).

Confocal Microscopy. Immunofluorescent labeling was visualized using an Olympus FV1000 confocal microscope. Analysis of muscle innervation was performed using CANJI, a custom image-analysis suite. Motor neuron, astrocyte, microglia, and interneuron analyses were performed using ImageJ (details are given in *SI Materials and Methods*).

Electrophysiology. The experimental procedures used to measure endplate currents at the mouse NMJ have been described previously (61). All electrophysiology was performed in muscles dissected from P100 mice (details are given in *SI Materials and Methods*).

Electron Microscopy. Tibialis anterior muscles were fixed with 4% PFA and 2.5% glutaraldehyde. Vibratome sections were processed using the sequential osmium tetroxide-thiocarbohydrazide-osmium (OTO) method as described previously (62) and were imaged by scanning electron microscopy (details are given in *SI Materials and Methods*).

Protein Analysis and Immunoprecipitation. Lumbar spinal cords were homogenized and separated into soluble and insoluble fractions by centrifugation. The soluble fraction was used for immunoprecipitation experiments, and protein levels were determined by Western blot (details are given in *SI Materials and Methods*).

Gene-Expression Analysis. RNA was isolated from lumbar spinal cords of P150 mice, and libraries were prepared using standard protocols before sequencing using the Illumina platform. ExpressionPlot (63) was used to generate two-way plots (details are given in *SI Materials and Methods*).

Statistics. Statistics for immunofluorescent, biochemical, and phenotypic analyses were performed using Prism v6.0f (GraphPad Software). ANOVA was followed by the appropriate post hoc tests as indicated.

ACKNOWLEDGMENTS. Excellent technical support was provided by Esther Kaunga, Sean O'Keeffe, Amy Kirner, and Angelica Struve. We thank Ai Yamamoto for her critical reading of the manuscript and Ai Yamamoto, David Sulzer, Jolene Windle, Neil Shneider, Robert Darnell, and members of their laboratories for reagents and advice. This study was supported by Project ALS, NIH Grant DP1 OD003930, and a grant from Takeda Pharmaceuticals. Additional support for N.D.R. came from National Institute of Neurological Disorders and Stroke (NINDS) Grant F31 NS089131 and NIH Medical Scientist Training Program Training Grant T32 GM007367; support for X.W. and M.M.R. came from NINDS Grant R01 NS082354.

1. Kanning KC, Kaplan A, Henderson CE (2010) Motor neuron diversity in development and disease. *Annu Rev Neurosci* 33:409–440.
2. Kim HJ, et al. (2013) Mutations in prion-like domains in hnRNPA2B1 and hnRNPA1 cause multisystem proteinopathy and ALS. *Nature* 495:467–473.
3. Kato M, et al. (2012) Cell-free formation of RNA granules: Low complexity sequence domains form dynamic fibers within hydrogels. *Cell* 149:753–767.
4. Taylor JP, Brown RH, Jr, Cleveland DW (2016) Decoding ALS: From genes to mechanism. *Nature* 539:197–206.
5. Cirulli ET, et al.; FALS Sequencing Consortium (2015) Exome sequencing in amyotrophic lateral sclerosis identifies risk genes and pathways. *Science* 347:1436–1441.
6. Weishaupt JH, Hyman T, Dikic I (2016) Common molecular pathways in amyotrophic lateral sclerosis and frontotemporal dementia. *Trends Mol Med* 22:769–783.
7. Ahmad L, Zhang SY, Casanova JL, Sancho-Shimizu V (2016) Human TBK1: A gatekeeper of neuroinflammation. *Trends Mol Med* 22:511–527.
8. Sullivan PM, et al. (2016) The ALS/FTLD associated protein C9orf72 associates with SMCR8 and WDR41 to regulate the autophagy-lysosome pathway. *Acta Neuropathol Commun* 4:51.
9. Webster CP, et al. (2016) The C9orf72 protein interacts with Rab1a and the ULK1 complex to regulate initiation of autophagy. *EMBO J* 35:1656–1676.
10. Mizushima N, Yoshimori T, Ohsumi Y (2011) The role of Atg proteins in autophagosome formation. *Annu Rev Cell Dev Biol* 27:107–132.
11. Mizuno Y, et al. (2006) Immunoreactivities of p62, an ubiqutin-binding protein, in the spinal anterior horn cells of patients with amyotrophic lateral sclerosis. *J Neurol Sci* 249:13–18.
12. Hernandez D, et al. (2012) Regulation of presynaptic neurotransmission by macroautophagy. *Neuron* 74:277–284.

13. Inoue K, et al. (2013) Coordinate regulation of mature dopaminergic axon morphology by macroautophagy and the PTEN signaling pathway. *PLoS Genet* 9:e1003845.
14. Tang G, et al. (2014) Loss of mTOR-dependent macroautophagy causes autistic-like synaptic pruning deficits. *Neuron* 83:1131–1143.
15. Zhang X, et al. (2011) Rapamycin treatment augments motor neuron degeneration in SOD1(G93A) mouse model of amyotrophic lateral sclerosis. *Autophagy* 7:412–425.
16. Castillo K, et al. (2013) Trehalose delays the progression of amyotrophic lateral sclerosis by enhancing autophagy in motoneurons. *Autophagy* 9:1308–1320.
17. Li Y, et al. (2015) Trehalose decreases mutant SOD1 expression and alleviates motor deficiency in early but not end-stage amyotrophic lateral sclerosis in a SOD1-G93A mouse model. *Neuroscience* 298:12–25.
18. Zhang X, et al. (2014) MTOR-independent, autophagic enhancer trehalose prolongs motor neuron survival and ameliorates the autophagic flux defect in a mouse model of amyotrophic lateral sclerosis. *Autophagy* 10:588–602.
19. Nassif M, et al. (2014) Pathogenic role of BECN1/Beclin 1 in the development of amyotrophic lateral sclerosis. *Autophagy* 10:1256–1271.
20. Fornai F, et al. (2008) Lithium delays progression of amyotrophic lateral sclerosis. *Proc Natl Acad Sci USA* 105:2052–2057.
21. Gill A, Kidd J, Vieira F, Thompson K, Perrin S (2009) No benefit from chronic lithium dosing in a sibling-matched, gender balanced, investigator-blinded trial using a standard mouse model of familial ALS. *PLoS One* 4:e6489.
22. Pizzasegola C, et al. (2009) Treatment with lithium carbonate does not improve disease progression in two different strains of SOD1 mutant mice. *Amyotroph Lateral Scler* 10:221–228.
23. Kaplan A, et al. (2014) Neuronal matrix metalloproteinase-9 is a determinant of selective neurodegeneration. *Neuron* 81:333–348.
24. Rogov V, Dötsch V, Johansen T, Kirkin V (2014) Interactions between autophagy receptors and ubiquitin-like proteins form the molecular basis for selective autophagy. *Mol Cell* 53:167–178.
25. Xie Y, et al. (2015) Endolysosomal deficits augment mitochondria pathology in spinal motor neurons of asymptomatic fALS mice. *Neuron* 87:355–370.
26. Mizushima N, Yamamoto A, Matsui M, Yoshimori T, Ohsumi Y (2004) In vivo analysis of autophagy in response to nutrient starvation using transgenic mice expressing a fluorescent autophagosome marker. *Mol Biol Cell* 15:1101–1111.
27. Le Grand JN, et al. (2013) Specific distribution of the autophagic protein GABARAPL1/GEC1 in the developing and adult mouse brain and identification of neuronal populations expressing GABARAPL1/GEC1. *PLoS One* 8:e63133.
28. Wang Y, et al. (2006) Distribution and ultrastructural localization of GEC1 in the rat CNS. *Neuroscience* 140:1265–1276.
29. Vlug AS, et al. (2005) ATF3 expression precedes death of spinal motoneurons in amyotrophic lateral sclerosis-SOD1 transgenic mice and correlates with c-Jun phosphorylation, CHOP expression, somato-dendritic ubiquitination and Golgi fragmentation. *Eur J Neurosci* 22:1881–1894.
30. Komatsu M, et al. (2005) Impairment of starvation-induced and constitutive autophagy in Atg7-deficient mice. *J Cell Biol* 169:425–434.
31. Zagoraiou L, et al. (2009) A cluster of cholinergic premotor interneurons modulates mouse locomotor activity. *Neuron* 64:645–662.
32. Tashiro Y, et al. (2012) Motor neuron-specific disruption of proteasomes, but not autophagy, replicates amyotrophic lateral sclerosis. *J Biol Chem* 287:42984–42994.
33. Pun S, Santos AF, Saxena S, Xu L, Caroni P (2006) Selective vulnerability and pruning of phasic motoneuron axons in motoneuron disease alleviated by CNTF. *Nat Neurosci* 9:408–419.
34. Schaefer AM, Sanes JR, Lichtman JW (2005) A compensatory subpopulation of motor neurons in a mouse model of amyotrophic lateral sclerosis. *J Comp Neurol* 490: 209–219.
35. Boillée S, et al. (2006) Onset and progression in inherited ALS determined by motor neurons and microglia. *Science* 312:1389–1392.
36. Yamanaka K, et al. (2008) Astrocytes as determinants of disease progression in inherited amyotrophic lateral sclerosis. *Nat Neurosci* 11:251–253.
37. Gal J, et al. (2009) Sequestosome 1/p62 links familial ALS mutant SOD1 to LC3 via an ubiquitin-independent mechanism. *J Neurochem* 111:1062–1073.
38. Phatnani HP, et al. (2013) Intricate interplay between astrocytes and motor neurons in ALS. *Proc Natl Acad Sci USA* 110:E756–E765.
39. Coffey ET (2014) Nuclear and cytosolic JNK signalling in neurons. *Nat Rev Neurosci* 15: 285–299.
40. Zhang Y, et al. (2014) An RNA-sequencing transcriptome and splicing database of glia, neurons, and vascular cells of the cerebral cortex. *J Neurosci* 34:11929–11947.
41. Cahoy JD, et al. (2008) A transcriptome database for astrocytes, neurons, and oligodendrocytes: A new resource for understanding brain development and function. *J Neurosci* 28:264–278.
42. Bandyopadhyay U, et al. (2013) RNA-Seq profiling of spinal cord motor neurons from a presymptomatic SOD1 ALS mouse. *PLoS One* 8:e53575.
43. Chiu IM, et al. (2013) A neurodegeneration-specific gene-expression signature of acutely isolated microglia from an amyotrophic lateral sclerosis mouse model. *Cell Rep* 4:385–401.
44. Williams ER, Baker SN (2009) Renshaw cell recurrent inhibition improves physiological tremor by reducing corticomuscular coupling at 10 Hz. *J Neurosci* 29:6616–6624.
45. Wootz H, et al. (2013) Alterations in the motor neuron-renshaw cell circuit in the Sod1(G93A) mouse model. *J Comp Neurol* 521:1449–1469.
46. Hultborn H, Katz R, Mackel R (1988) Distribution of recurrent inhibition within a motor nucleus. II. Amount of recurrent inhibition in motoneurones to fast and slow units. *Acta Physiol Scand* 134:363–374.
47. Komatsu M, et al. (2007) Essential role for autophagy protein Atg7 in the maintenance of axonal homeostasis and the prevention of axonal degeneration. *Proc Natl Acad Sci USA* 104:14489–14494.
48. Maday S, Wallace KE, Holzbaur EL (2012) Autophagosomes initiate distally and mature during transport toward the cell soma in primary neurons. *J Cell Biol* 196: 407–417.
49. Shen W, Ganetzky B (2009) Autophagy promotes synapse development in Drosophila. *J Cell Biol* 187:71–79.
50. Ravits JM, La Spada AR (2009) ALS motor phenotype heterogeneity, focality, and spread: Deconstructing motor neuron degeneration. *Neurology* 73:805–811.
51. Braak H, et al. (2013) Amyotrophic lateral sclerosis–A model of corticofugal axonal spread. *Nat Rev Neurol* 9:708–714.
52. Stephens B, et al. (2006) Widespread loss of neuronal populations in the spinal ventral horn in sporadic motor neuron disease. A morphometric study. *J Neurol Sci* 244:41–58.
53. Hossaini M, et al. (2011) Spinal inhibitory interneuron pathology follows motor neuron degeneration independent of glial mutant superoxide dismutase 1 expression in SOD1-ALS mice. *J Neuropathol Exp Neurol* 70:662–677.
54. Morrison BM, Janssen WG, Gordon JW, Morrison JH (1998) Time course of neuropathology in the spinal cord of G86R superoxide dismutase transgenic mice. *J Comp Neurol* 391:64–77.
55. Virgo L, de Belleroche J (1995) Induction of the immediate early gene c-jun in human spinal cord in amyotrophic lateral sclerosis with concomitant loss of NMDA receptor NR-1 and glycine transporter mRNA. *Brain Res* 676:196–204.
56. Sun S, et al. (2015) Translational profiling identifies a cascade of damage initiated in motor neurons and spreading to glia in mutant SOD1-mediated ALS. *Proc Natl Acad Sci USA* 112:E6993–E7002.
57. Nilsson P, et al. (2013) Aβ secretion and plaque formation depend on autophagy. *Cell Rep* 5:61–69.
58. Ejlerskov P, et al. (2013) Tubulin polymerization-promoting protein (TPPP/p25α) promotes unconventional secretion of α-synuclein through exophagy by impairing autophagosome-lysosome fusion. *J Biol Chem* 288:17313–17335.
59. Baixauli F, López-Otín C, Mittelbrunn M (2014) Exosomes and autophagy: Coordinated mechanisms for the maintenance of cellular fitness. *Front Immunol* 5:403.
60. Guo JL, Lee VM (2014) Cell-to-cell transmission of pathogenic proteins in neurodegenerative diseases. *Nat Med* 20:130–138.
61. Wang X, et al. (2004) Decreased synaptic activity shifts the calcium dependence of release at the mammalian neuromuscular junction in vivo. *J Neurosci* 24:10687–10692.
62. Tapia JC, et al. (2012) High-contrast en bloc staining of neuronal tissue for field emission scanning electron microscopy. *Nat Protoc* 7:193–206.
63. Friedman BA, Maniatis T (2011) ExpressionPlot: A web-based framework for analysis of RNA-Seq and microarray gene expression data. *Genome Biol* 12:R69.